RSC Advances

ROYAL SOCIETY OF CHEMISTRY

www.rsc.org/advances

A sensitive cataluminescence-based sensor using $SrCO_3$/graphene composite for n-propanol

Qianchun Zhang*, Feifei Meng, Lin Zha, Xingyi Wang and Guoyi Zhang

Abstract: In this paper, we developed a cataluminescence-based sensor using $SrCO_3$/graphene for sensitive and selective detection of n-propanol. The characterization the composite were performed by X-ray diffraction (XRD), transmission electron microscopy (TEM), fourier transform infrared (FT-IR) spectra and gas adsorption instrument. The sensor was successfully applied to sensing *n*-propanol in liquid samples by coupling a miniature vaporizing device with the sensor cell. The experimental results revealed that the $SrCO_3$/graphene sensor exhibited about 5.8 times higher sensitivity than that of pure $SrCO_3$, indicating that sensitivity of $SrCO_3$/graphene sensor for *n*-propanol detection was enhanced by adding graphene into $SrCO_3$. The linear range of the fabricated sensor was 0.2 to 32 mg L^{-1} (r = 0.9987) with a limit of detection (LOD) of 0.08 mg L^{-1}. The sensor showed fast rapid response and recovery times of 2 s and 20 s, respectively. The sensor was used to analyze samples spiked with known concentrations of *n*-propanol. The concentrations of *n*-propanol in all samples were well quantified with satisfactory recoveries, thereby indicating the $SrCO_3$/graphene based sensor was a promising candidate for fast, sensitive and selective detection of n-propanol. The possible

School of Biology and Chemistry, Xingyi Normal University for Nationalities, Xingyi, 562400, People's Republic of China

* Corresponding author: Tel: +86-589-3296359; Fax: +86-859-3527567

E-mail: qianchunzhang@qq.com

mechanism was also discussed on the basis of the reaction products.

1. Introduction

Graphene with a two-dimensional monolayer of fused sp^2 carbon bonds in a honeycomb-like network, has attracted a great deal of scientific interest in the area of chemical gas sensing, which is mainly attributed to its outstanding mechanical, electrical, thermal, and optical properties and large specific surface area.[1-4] Graphene is an ideal choice for decorating with other materials, including metal oxides, metal sulphides and metal nanoparticles for improved properties.[5-7] It was reported that the mixing of graphene into other materials not only can enhance the sensitivity and improve the selectivity of the composite, but also can reduce the operating temperature.[8-10] For example, Singh et al. reported that the sensors based on ZnO decorated graphene can sensitively detect the industrial gases such as CO, NH_3 and NO at room temperature.[11] Liu et al. have reported that mixing of graphene into $ZnFe_2O_4$ can reduce the operating temperature of the sensors for acetone.[12]

Cataluminescence (CTL) is an interest luminescent emission produced during the catalytic oxidation reaction of analyte molecule on the surface of solid catalyst.[13-15] CTL has attracted a great deal of research interest in the development of chemical sensor for the determination and discrimination of analytes.[16-19] The CTL-based gas sensor possesses many outstanding advantages such as good selectivity, high sensitivity, rapid response speed, good reproducibility and simple instrument.[20-22] The sensing element of CTL sensor is solid catalyst that is inconsumable during the sensing process, leading to this kind of chemical sensor has a long-term stability.[23-24]

To date, a lot of different kinds of materials have been applied to the development of CTL-based sensor. Examples include an iso-butanol sensor based on Y-doped metal-organic framework-5,[25] an n-hexane sensor based on Zeolite,[26] a nanosized ZrO_2-based sensor for propionaldehyde,[27] and nano-$3TiO_2$–$2BiVO_4$-based sensor for simultaneous determination of benzene and formaldehyde.[28] Lv' group reported a facile hydrothermal assisted in situ synthesis route for the preparation of graphene sheets decorated with SnO_2. The SnO_2/graphene composite was found to be a highly efficient material for CTL sensor to propanal.[29] This research group also reported a facile catalyst-free atmospheric pressure chemical vapour deposition method for the growth of hierarchical SnO_2 architectures on graphene.[7] It was found that the materials prepared by this method showed enhanced CTL response to methanol and a morphology-dependent CTL performance.

N-propanol is a colorless, flammable, fragrant liquid with moderately toxic, and is ubiquitous in nature. It is an important solvent principally used in printing, cosmetics, making leather product, and pesticides.[30] In addition, n-propanol is the major higher alcohols found in alcoholic beverages for it is widely used as flavor volatile in food and beverage manufacturing.[31] However, exposure to n-propanol can irritate the skin causing a rash or burning feeling on contact, and higher exposures can cause headache, dizziness, confusion, nausea and vomiting, and even liver damage.[32] Moreover, n-propanol is a flammable liquid and a dangerous fire hazard that will cause an explosion when it meets open flame. Recently, increasing concerns have been focused on the levels of higher alcohols include n-propanol in surrogate alcohol

(i.e., illicit or home-produced alcoholic beverages) that might result in an increased incidence of liver diseases in regions where there is a high consumption of such beverages.[31] Therefore, the development of sensor for n-propanol has wide application in environmental monitoring and foodstuff control.

In this work, we found that the $SrCO_3$ doped with 12 wt% graphene exhibited about 5.8 times CTL response to n-propanol than that of pure $SrCO_3$. A CTL-based sensor using $SrCO_3$/graphene was designed for sensitive and selective detection of n-propanol. Although graphene has been wildly used in the design of electrochemical sensors, only a few studies on its applications in CTL sensors were reported. Moreover, the previous CTL-based sensors were usually used for gaseous sample analysis. In order to expand of the detectable samples, a miniature vaporizing device was couple with the sensor cell for analysis of n-propanol in liquid sample. In this context, this paper was focused on the liquid sample sensing. The performance of the sensor was evaluated systematically in terms of response and recovery times, selectivity to n-propanol, and stability. The factors influencing the sensor for the determination of n-propanol were optimized in detail. The potential application of the sensor was demonstrated by the determination of n-propanol in spiked samples. Results showed that the sensor provided a simple, rapid, sensitive way for the determination of n-propanol.

2. Experimental

2.1 Chemicals and materials

All chemicals used in our experiments were of analytical grade. Methanol,

ethanol, ethyl acetate, n-hexane, formaldehyde, carbon tetrachloride, chloroform, propionaldehyde , acetaldehyde, 2-propanol, acetone were purchased from Damao Chemical Reagent Company (Tianjin, China). N-heptane, n-octane and iso- octane was supported by Fuyu Fine Chemical Co. Lit. (Tianjin, China). Sulfuretted hydrogen (500 ppm) was purchased from Zhandong Gas limited company (Chongqing, China). Graphite powder (particle size 300~500 nm) was purchased from Alfa Aesar. $SrCO_3$ was supplied by XinxinYuan Chemical Co., Ltd. (Sichuan, China). Other chemicals were obtained from Aladdin Chemical Co., Ltd. (Shanghai, China).

2.2 Materials preparation and characterization

Graphene was synthesized by hydrazine reduction of graphene oxide (GO). The GO was prepared by the oxidation of graphite powder with $H_2SO_4/KMnO_4$ according to the modified Hummer's method,[33-34] which resulted in water-soluble GO. Then, 0, 3, 12, 24, 30, 36, 45 and 54 mg of GO was dispersed in distilled water under ultrasonication condition to form colloidal suspensions. Subsequently, 0.3 g of $SrCO_3$ powder was direct added to prepare composite contains different mass percent of graphene. After 30 min of ultrasonic treatment, hydrazine monohydrate was added into these solutions, then ultrasonication for 30 min, followed by reflux at 90 ˚C for 6 h to ensure the complete reductionof GO. The solid products were collected by filtered through 0.45 mm filter and washed with distilled water until its filtrate became neutral. The precipitate was dried at 80 ˚C for 24 h under vacuum.

The morphologies of the materials were characterized with a transmission electron microscope (TEM, Tecnai™G2 Spirit) at an accelerating voltage of 120 kV.

X-ray power diffraction (XRD) experiments were carried out in a Thermo-VG Scientific ESCALAB 250 diffractometer. Fourier transform infrared (FT-IR) spectra were measured by Nicolet Avatar 330. Surface area measurements were performed on an ASAP-2020M gas adsorption instrument (Micromeritics, Atlanta, USA) at 77K.

2.3 CTL sensor fabrication and measurement

Fig. 1 shows the schematic diagram of the fabricated sensor device. 0.1 g of $SrCO_3$/graphene composite was deposited onto a cylindrical ceramic heater (length= 10 cm, diameter=0.6 cm) to form a catalyst layer. The ceramic heater was linked up with a voltage controller (Power □, Model: TG1783SL3A, Tonggao Electronic Co., Ltd., Ningbo, China). The temperature of the ceramic heater can be controlled by adjusting the output voltage of the voltage controller. The CTL sensor cell was constructed by inserting the ceramic heater into a home-made quartz tube (length= 9 cm, inner diameter=1 cm, outer diameter=1.2 cm) with inlet and outlet. A miniature PTC vaporizing device (power: 60 W, working voltage: 24 V, length of central cylinder=2.5 cm, diameter of central cylinder=2 cm, length of cylinder joint=1.5 cm, diameter of cylinder joint =0.6 cm, customized from Dongsheng Electronic Heating and Appliance Factory, Taizhou, China) was coupled with the sensor cell. The vaporizing device was linked up with another voltage controller (Power □). In the present work, 5 μL of liquid sample was injected into the vaporizing device. The liquid sample was vaporized immediately once it was injected into the vaporizing device, and then was driven towards the sensor cell by an airstream supplied by an air pump. A BPCL Ultra Weak Chemiluminescence Analyzer (Biophysics Institute of

Chinese Academy of Science, China) equipped with a photomultiplier (PMT) was used to record the CTL intensity. The detecting wavelengths could be selected over the range of 350–550 nm by changing the optical filters.

The data acquisition time for each signal point was set as 0.5 s, and the voltage for the photomultiplier tube was 850 V. The data was recorded with a computer and further processed with OriginPro. The response of the n-propanol sensor is defined as:

$$S=I-N \qquad (1)$$

Where S is the real response of the sensor, I stands for the recorded CTL intensity, and N is the background noise. The signal to noise (S/N) at 3 was used to reflect the limit of detection (LOD) of the sensor.

2.4 Instrumental analysis for mechanism study

In order to explore the possible reaction mechanism behind the n-propanol on the $SrCO_3$/graphene composite, an Agilent 7890A GC-MS equipped with a HP-INNO Wax column (30 m, 0.25 mm inner diameter, and 0.25μm film thickness) were used to analyze the products from the catalytic oxidation. The exhaust gas from the catalytic oxidation was collected into a sampling bag, and then 200 μL of the sample was injected into the instrument.

3. Results and discussion

3.1 Characterization of sensing material

Fig. 2a shows the FT-IR spectra of pristine graphite powder, GO, graphene, $SrCO_3$ and $SrCO_3$/graphene. The spectra reveal that after oxidation of graphite, the GO contains several functional groups includes OH (3432 cm^{-1}), COOH (1724 cm^{-1}),

and C=O (1625 cm^{-1}). Upon reduction of graphene oxide to graphene, the C=O band disappears and new bands at 2988 and 2865 cm^{-1} arise representing the C-H stretch vibrations of the methylene group. Similar results have been reported by Naebe et al.[35] The band at 1474 of IR spectrum for $SrCO_3$ corresponds to the asymmetric stretching mode of C-O bond. The sharp peaks at and 857 and 702 cm^{-1} are in plane and out plane bending CO_3^{2-}. The peaks of graphene are almost cannot be observed in the IR spectrum for $SrCO_3$/graphene, possibly due to less active group of graphene and its content is relative low in the $SrCO_3$/graphene composite.

Fig. 2b shows the XRD patterns of pristine graphite powder, GO, graphene, $SrCO_3$ and $SrCO_3$/graphene composite. A sharp intensive peak observed at the (002) diffraction line (d-spacing of 0.35 nm at 26.35°) and a weak (004) diffraction peak at 54.6° is highly specific for the nature of graphite powder. GO shows a diffraction peak at 2θ of 10.6° corresponding to a d-spacing of 0.8 nm. The diffraction peak at about 10.6° of GO is weaker than that of pristine graphite at about 26.35°, which confirms the successful oxidation of pristine graphite to be converted to GO. Compared with the pristine graphite, the (002) peak of graphene is decreased in its intensity and the distance is enlarged. The XRD pattern of $SrCO_3$ is in good agreement with orthorhombic $SrCO_3$ (strontianite, JCPDS: 05-0418). The XRD peak of $SrCO_3$/graphene composite indicates the intensity of $SrCO_3$ peak is low as compared to the characteristic peaks of pure $SrCO_3$ because of low content and low diffraction intensity of $SrCO_3$, while the peaks of GO is disappeared. Xu et al. have reported that if regular stacks of graphite oxide or graphite are destroyed, for example,

by exfoliation, then their diffraction peaks become weak or may even disappear.[36] Therefore, the disappearance of the peaks of graphene can be attributed to exfoliation of GO sheet.

Fig. 3 shows TEM images of the graphene, $SrCO_3$ and $SrCO_3$/graphene composite, respectively. As shown in Fig. 3a, a mixture of few layer graphene with flakes-like structures is observed to be situated on the top of the copper grid. The TEM micrograph of $SrCO_3$ shown in Fig. 3b indicates that the $SrCO_3$ is orthogonal crystal, which is consistent with the result of XRD experiment. It can be seen from the Fig. 3c that the $SrCO_3$ is decorated successfully with graphene, and is partially intercalated between two graphene sheets. The specific surface areas of $SrCO_3$, graphene and $SrCO_3$/graphene are measured by N_2 (77.4 K) adsorption and desorption isotherms. The results show that the specific surface areas of $SrCO_3$, graphene and $SrCO_3$/graphene are 37, 786 and 104 $m^2 g^{-1}$, respectively. An obvious enhanced specific surface area of $SrCO_3$/graphene composite was observed compare with pure $SrCO_3$.

3.2 Optimization

3.2.1 Doping concentration

We found that n-propanol cannot produce CTL response on pure graphene, but can produce CTL response on $SrCO_3$, the addition of graphene into $SrCO_3$ can enhance the sensitivity for n-propanol. These results demonstrate that $SrCO_3$ is used as a catalyst while graphene is used as a sensitizer during the CTL detection of n-propanol. Fig. 4a shows the CTL responses for n-propanol using $SrCO_3$ and $SrCO_3$

doped with 12 wt% graphene as sensing materials. The CTL response for n-propanol on $SrCO_3$/graphene composite is about 5.8-fold stronger than that of pure $SrCO_3$. The relative standard deviation (RSD) of five times responses for n-propanol on $SrCO_3$/graphene composite is 3.4%, indicating that the $SrCO_3$/graphene composite is an optional sensing material with stable reproducibility for the determination of n-propanol .

Fig. 4b shows the CTL intensity versus $SrCO_3$ with different doping concentrations of graphene. It can be seen that the CTL intensity increases monotonically with increasing doping concentrations of graphene before 12 wt%. It is clear that $SrCO_3$ doped with 12 wt% graphene exhibits the best response, and was subsequently chosen for further sensing characterizations.

3.2.2 Vaporized and detecting temperature

Fig. 5a shows the CTL signal versus different vaporized temperatures under fixing detecting temperature of 245°C condition. It can be seen that the optimal vaporized temperature is 120 °C. We found that the liquid sample containing n-propanol could not be completely vaporized at low temperature resulted in broad peaks on the response curves. However, as Fig. 5a shows, the CTL intensity decreases with increasing of vaporized temperature above 120 °C, possibly due to the n-propanol was already decomposed in part before reaching the sensor cell.

Fig. 5b shows the CTL intensity, background noise and S/N versus detecting temperature under fixing vaporized temperature at 120 °C condition. It can be seen that the CTL signal increases with the increasing of detecting temperature and reaches

to its maximum at 258 °C. However, the background noise that mainly results from the thermal radiation of the heated sensing material also increases with increase of temperature, which leads to S/N decreasing significantly at high temperature Therefore, the temperature of 245 °C was chosen as the optimum detecting temperature since the S/N ratio was reaches its maximum at this temperature.

3.2.3 Wavelength and flow rate

Fig. 6a shows the CTL intensity, background noise and S/N versus with wavelength at a flow rate of 260 mL min^{-1}. Although the strongest emission is observed at 440 nm, the background noise increases dramatically with the increase of wavelength, leading to the maximum S/N is observed at 425 nm. Therefore, 425 nm was selected as the optimum wavelength for the quantitative detection of n-propanol.

Fig. 6b shows the change trend of the CTL intensity versus flow rate at 425 nm. The result shows that the catalytic oxidation reaction of n-propanol is controlled by diffusion rate below 260 mL min^{-1}, which is the total reaction rate is controlled by the rate of the transfer of n-propanol molecular from the gas phase to the catalyst surface, leading to the CTL intensity is proportional to flow rate. However, the total reaction rate of n-propanol is limited by the oxidation rate of n-propanol on the catalyst surface when the flow rate above 260 mL min^{-1}, resulting in CTL intensity is independent of the flow rate. Therefore, the flow rate of 260 mL min^{-1} was chosen as the optimal flow rate for the subsequent work.

3.3 The performance of the sensor

3.3.1 Response and recovery times

The response time and recovery time are important indicators for evaluating the performance of the sensor for rapid detection. The response time is defined as the time needed to reach the maximum value from the injection, and the recovery time is defined as the time needed to decay to the background noise from the maximum value. Fig. 7a shows the response of the sensor to different concentrations of n-propanol from 6.4 to 16 mg L^{-1}. It can be seen that the CTL response profiles are similar to each other. For all three concentrations of n-propanol, the maximum signals were achieved at around 2 s after injection, indicating a rapid response of the sensor to different concentrations of n-propanol. We can see that the recovery time increases slightly with the increasing of the n-propanol concentration, and the recovery time of the sensor to n-propanol at a concentration of 16 mg L^{-1} is about 20 s, which represent the fast recovery capacity of the sensor.

3.3.2 Selectivity and stability

Selectivity is a very important performance indicator for a sensor, as poor selectivity prone to the generation of false positives. In order to evaluate the selectivity of the sensor towards n-propanol, in total of 24 common compounds at concentration of 10 mg L^{-1} except gaseous hydrogen sulfide at 500 ppm were injected into the sensor. Additionally, 1 mL of liquefied petroleum gas (LPG) mainly consists of butane and pentane was also injected into the sensor to evaluate to selectivity of the sensor. As shown in Fig. 7b, although propionaldehyde will produce strong response, only weak or no responses from other compounds are observed, thus the sensor based on $SrCO_3$/graphene composite has an acceptable selectivity towards n-propanol. It

was reported that the size, shape and morphology of the catalyst have great effects on the CTL performances,[16] leading to the same type of catalysts with different characterizations show different CTL performances for different compounds. For example, vinyl acetate can induce strong CTL response on nanosized MgO,[37] but very weak CTL response on MgO film.[38] $SrCO_3$ also was used as catalyst for CTL detection of H_2S,[39] however, only very weak CTL response was observed when H_2S passed through the $SrCO_3$/graphene composite, which possibly also results from the characterizations of previous reported $SrCO_3$ are different from the $SrCO_3$/graphene used at the present work.

The sensor was stored at room temperature, and the effect of storage time on the stability was investigated by measuring the CTL intensity of n-propanol at a concentration of 10 mg L^{-1} per 24 h for one week. We found that the sensor exhibited long-term stability with a RSD of 6.5% for seven replicate determinations during one week of periodic operations.

3.5. Analytical figures of merit

Fig. 8 shows the CTL response versus the different concentrations of n-propanol under the optimized conditions. A linear relationship was found between the CTL intensity and n-propanol concentration ranging 0.2 to 32 mg L^{-1}. The linear equation for the $SrCO_3$/graphene-based n-propanol sensor was characterized by $I = 414.5C + 104.9$ (correlation coefficient $r = 0.9989$), where I is the relative CTL intensity and C is the concentration of n-propanol. The LOD at an S/N of 3 is 0.08 mg L^{-1}.

3.6 Sample analysis

In order to evaluate the analytical application of the sensor, samples spiked with known concentrations of n-propanol were prepared for recovery experiments. Because n-propanol, benzaldehyde and β-phenylethanol are common used as flavouring agents in food manufacturing; n-propanol are commonly found in alcoholic beverages. Therefore, solution comprises isopyknic of benzaldehyde (10 mg L^{-1}) and β-phenylethanol (10 mg L^{-1}) was selected as sample 1, and Tsingtao beer (alcohol content: 2.5%) was selected as sample 2. The two kinds of sample were spiked with n-propanol standard at three levels of 1, 5 and 10 mg L^{-1} for recovery experiments. As shown in Table 1, the recoveries for n-propanol in different samples were 82.4–116.5% with the RSDs of 5.7–10.4%, respectively, thereby indicating the utility of the sensor for rapid detection of n-propanol in real sample.

3.7 Possible mechanism

According to widely accepted theory about CL reaction, excited intermediates would be formed during the catalytic oxidation of n-propanol. The luminescence emission could be produced when the excited intermediates falling to ground state. In order to study the mechanism, GC–MS experiments were performed to indentify the reaction products of the catalytic oxidation of n-propanol on $SrCO_3$ and $SrCO_3$/graphene composite. As Fig. 9 shows, the catalytic oxidations of n-propanol on both $SrCO_3$ and $SrCO_3$/graphene composite yield n-propanal, acetaldehyde and carbon dioxide, indicating that the enhanced CTL intensity does not result from the new products, n-propanol undergoes the same reaction path on $SrCO_3$ and $SrCO_3$/graphene. It can be seen that the residual amounts of n-propanol,

propionaldehyde and acetaldehyde on $SrCO_3$/graphene are less than that of on $SrCO_3$, while the amounts of carbon dioxide on $SrCO_3$/graphene is higher than that of on $SrCO_3$, which indicates that efficiency of catalytic oxidation for $SrCO_3$/graphene is higher than that of pure $SrCO_3$. The experiments show that the specific surface area of $SrCO_3$/graphene is larger than that of pure $SrCO_3$, which may the possible reason for the enhanced efficiency of catalytic oxidation for $SrCO_3$/graphene composite.

The formation of propionaldehyde during catalytic oxidation might be thought to suggest the initial point of attack in n-propanol by oxygen occurs mainly at the α-C-H and O-H bonds. The formation of copious amount of carbon dioxide suggests that it is the possible final product. The Fig 7b shows that propionaldehyde can produce strong CTL signal, and acetaldehyde can produce weak CTL signal on $SrCO_3$/graphene composite. It was reported that acetaldehyde and carbon dioxide at the excited states are the important luminous intermediates generated during the CTL reaction process.[40-41] Therefore, the oxidations of propionaldehyde and acetaldehyde during the oxidation of n-propanol process are supposed to the mainly responsible for the CTL emission. According to these results, the possible mechanism of oxidation of n-propanol could be described as the following reactions: oxygen molecule is absorbed by the catalyst to form active oxygen molecule (reaction 1); propionaldehyde then is formed from the reaction of the resulting n-propanol with oxygen (reaction 2); propionaldehyde is oxidized to produce acetaldehyde and carbon dioxide, accompanied by strong photoemission (reaction 3); acetaldehyde is oxidized to produce carbon dioxide, which generates weak photoemission (reaction 4).

$$O_2 \xrightarrow[\text{Catalyst}]{\triangle} 2O \quad (1)$$

$$CH_3CH_2CH_2OH + O \xrightarrow[\text{Catalyst}]{\triangle} CH_3CH_2CHO + H_2O \quad (2)$$

$$CH_3CH_2CHO + 3O \xrightarrow[\text{Catalyst}]{\triangle} CH_3CHO + CO_2 + H_2O + hv \quad (3)$$

$$CH_3CHO + 5O \xrightarrow[\text{Catalyst}]{\triangle} 2CO_2 + 2H_2O + hv \quad (4)$$

The Cullis et al. reported that the gaseous oxidation of n-propanol shows considerable similarity to that of ethanol, both of them are to form corresponding aldehydes at their initial reaction periods. The principal difference then between the oxidation of 2-propanol and the corresponding reaction of the primary alcohols is that ketone replaces aldehyde as the main initial reaction product.[42] They stated that the α-C-H bond should be more reactive in n-propanol than in ethanol since the electron-repelling CH_3 group is further removed from the point of attack, and the relative reactivities of ethanol, n-propanol and 2-propanol toward oxygen is n-propanol > ethanol > 2-propanol. Possibly for the different reaction paths between n-propanol and 2-propanol, and the higher reactivity of n-propanol results in n-propanol produces higher CTL signal that that of ethanol and 2-propanol on $SrCO_3$/graphene composite (Fig. 7b). However, further work should be done to better understand the mechanism of CTL reaction n-propanol on $SrCO_3$/graphene composite.

4. Conclusion

In summary, the $SrCO_3$/graphene composite has been synthesized to fabricated n-propanol sensor. The effect of the graphene loading concentrations of $SrCO_3$ on sensing property of n-propanol was investigated. It was concluded that the existence

of graphene in the composite enhanced the sensitivity of the composite toward n-propanol, and optimum amount of graphene content at 12 wt% has been found for the fabrication of n-propanol sensor. By coupling with a miniature vaporizing device, the sensor was successfully applied to the analysis of n-propanol in liquid samples, which expanded the range of detectable sample. The detecting conditions of the sensor include vaporized temperature, detecting temperature, wavelength, and flow rate for the determination of n-propanol were systematically optimized. The sensor was successfully applied to the determination of n-propanol in spiked samples. The recoveries were 82.4–116.5% with the RSDs of 5.7–10.4%, respectively. Finally, the possible reaction mechanism behind the n-propanol on the $SrCO_3$/graphene composite was also studied by GC-MS experiments. It should be noted that the sensor is not limit to the determination of n-propanol in liquid samples, it also can be used for rapid sensing gaseous n-propanol. Therefore, our work provides a selective, sensitive and convenient method for rapid determination of n-propanol.

Acknowledgements

This study was supported by the Science and Technology Foundation of the Guizhou Provincial Science and Technology Department (No. LH20147406), the Natural Science Foundation of the Guizhou Provincial Education Department (No. 2012070), and the Social Development Foundation of the Science and Technology Bureau of Qianxinan Prefecture (No. 201430).

References

1 K. Novoselov, A. K. Geim, S. Morozov, D. Jiang, M. K. I. Grigorieva, S. V. Dubonos and A. A. Firsov, *Nature*, 2005, **438**, 97-200.

2 H. Pei, J. Li, M. Lv, J. Y. Wang, J. M. Gao, J. X. Lu, Y. P. Li, Q. Huang, J. Hu and C. H. Fan, *J. Am. Chem. Soc.*, 2012, **134**, 13843-13849.

3 R. K. Paul, S. Badhulika, N. M. Saucedo and A. Mulchandani, *Anal. Chem*., 2012, **84**, 8171-8178.

4 Y. Y. Su and Y. Lv, *RSC Adv*., 2014, **4,** 29324-29339.

5 D. Z. Zhang, J. Q. Liu, H. Y. Chang, A. M. Liu and B. K. Xia, *RSC Adv*., 2015, **5**, 18666-18672.

6 P. G. Su and S. L. Peng, *Talanta*, 2015, **132**, 398-405.

7 L. Z. Yu, L. C. Zhang, H. J. Song, X. M. Jiang and Y. Lv, *CrystEngComm*, 2014, **16**, 3331-3340.

8 Y. X. Liu, X. C. Dong and P. Chen*, Chem. Soc. Rev*. 2012, **6**, 2283-2307.

9 F. Yavari and N. Koratkar, *J. Phys. Chem. Lett*., 2012, **3**, 1746-1753.

10 W. J. Yuan and G. Q. Shi, *J. Mater. Chem. A*, 2013, **1**, 10078-10091.

11 G. Singh, A. Choudhary, D. Haranath, A. G. Joshi, N. Singh, S. Singh and R. Pasricha, *Carbon*, 2012, **50**, 385-394.

12 F. Liu, X. F. Chu, Y P. Dong, W. B. Zhang, W. S. Sun and L. M. Shen, *Sens. Actuators B,* 2013, **188**, 469-474.

13 Y. F. Zhu, J. J. Shi, Z. Y. Zhang, C. Zhang and X. R. Zhang, *Anal. Chem.*, 2002, **74**, 120-124.

14 T. Okabayashi, T. Fujimoto, I. Yamamoto, K. Utsunomiya, T. Wada, Y. Yamashita, N. Yamashita and M. Nakagawa, *Sens. Actuators B*, 2000, **64**, 54-58.

15 J. Z. Zheng, W. X. Zhang, J. Cao, X. H. Su, S. F. Li, S. R. Hu, S. X. Li and Z. M. Rao, *RSC Adv*. 2014, **4**, 21644-21649.

16 N. Na, S. C. Zhang, S. Wang and X. R. Zhang, *J. Am. Chem. Soc*., 2006, **128**, 14420-14421.

17 Y. Wu, N. Na, S. C. Zhang, X. Wang, D. Liu and X. R. Zhang, *Anal. Chem.*, 2009, **81**, 961-966.

18 R. K. Zhang, Y. F. Hu and G. K. Li, *Anal. Chem.*, 2014, **86**, 6080-6087.

19 R. K Zhang, X. A. Cao, Y. H. Liu and X. Y. Chang, *Anal. Chem.*, 2013, **85**, 3802-3806.

20 L. J. Zhang, W. Q. Rong, Y. C. Chen, C. Lu and L. X. Zhao, *Sens. Actuators B*, 2014, **205**, 82-87.

21 J. Y. Han, F. F. Han, J. Ouyang, L. X. He, Y. T. Zhang and N. Na, *Nanoscale*, 2014, 6, 3069-3072.

22 L. Xu, H. J. Song, J. Hu, Y. Lv and K. L. Xu, *Sens. Actuators B*, 2012, **169**, 261-266.

23 W. F. Niu, H. Kong, H. Wang, Y. T. Zhang, S. C. Zhang and X. R. Zhang, *Anal. Bioanal. Chem*., 2012, **402**, 389-395.

24 H. L. Zhang, L. C. Zhang, J. Hu, P. Y. Cai and Y. Lv, *Talanta*, 2010, **82**, 733-738.

25 X. Y. Wan, H. J. Song, D. Zhao, L. C. Zhang and Y. Lv, *Sens. Actuators B*, 2014, **201**, 413-419.

26 P. Yang, X. N. Ye, C. W. Lau, Z. X. Li, X. Liu and J. Z. Lu, *Anal. Chem*., 2007, **79**, 1425-1432.

27 Y. X. Chu, Q. C Zhang, Y. H. Li, Z. M. Xu and W. R. Long, *Microchim. Acta.*, 2014, **181**, 1-8.

28 K. W. Zhou, Y. L. Cheng, H. W. Yang, C. X. Gu, Y. Xiao and M. H. Zhao, *Sens. Actuators B*, 2014, **202**, 721-726.

29 H. J. Song, L. C. Zhang, C. L. He, Y. Qu, Y. F. Tian and Y. Lv, *J. Mater. Chem*., 2011, **21**, 5972-5977.

30 Inert Reassessment-n-Propanol. WASHINGTON, D.C. 20460 office of prevention pesticides, and toxit substances, http://www.epa.gov/opprd001/inerts/propanol.pdf, (accessed August 2005).

31 D. W. Lachenmeier, S. Haupt, K and Schulz, *Regul. Toxico.l Pharm*., 2008, **50**, 313-321.

32 New jersey department of health and senior services. Hazardous substance fact sheet, http://nj.gov/health/eoh/rtkweb/documents/fs/1605.pdf. (accessed May 2005).

33 B. Gulbakan, E. Yasun, M. I. Shukoor, Z. Zhu, M. X. You, X. H. Tan, H. Sanchez, D. H. Powell, H.J. Dai and W. H. Tan, *J. Am. Chem. Soc*., 2010, **132**, 17408-17410.

34 V. K. Ponnusamy and J. F. Jen, *J. Chromatogr. A*, 2011, **1218**, 6861-6868.

35 M. Naebe, J. Wang, A. Amini, H. Khayyam, N. Hameed, L. H. Li, Y. Chen and B. Fox, *Sci. Rep*., 2014, **4**, 1-7.

36 C. Xu, X. Wang and J. W. Zhu, *J. Phys. Chem. C*, 2008, **112**, 19841-19845.

37 C.C. Wu, X. A. Cao, Q. Wen, Z. H. Wang, Q. Q. Gao and H.C. Zhu, *Talanta*, 2009, **5**, 1223-1227.

38 Y. Tao, X. A. Cao, Y. Peng and Y. H. Liu, *Sens. Actuators B*, 2010, **1**, 292-297.

39 Y. H. Liu, F. Tang, C. J. Kang and X. A. Cao, *Luminescence*, 2012, 4, 274-278.

40 Z. Y. Zhang, K. Xu, W. R. G. Baeyens and X. R. Zhang, A*nal. Chem. Acta*. 2005, **1**, 145-152.

41 X. Wang, N. Na, S. C. Zhang, Y. Y. Wu and X. R. Zhang, *J. Am. Chem. Soc*., **19**, 6062-6063.

42 C. F. Cullis and E. J. Newitt, *Proc. R. Soc. London, Ser. A*, 1960, **1290**, 402-412.

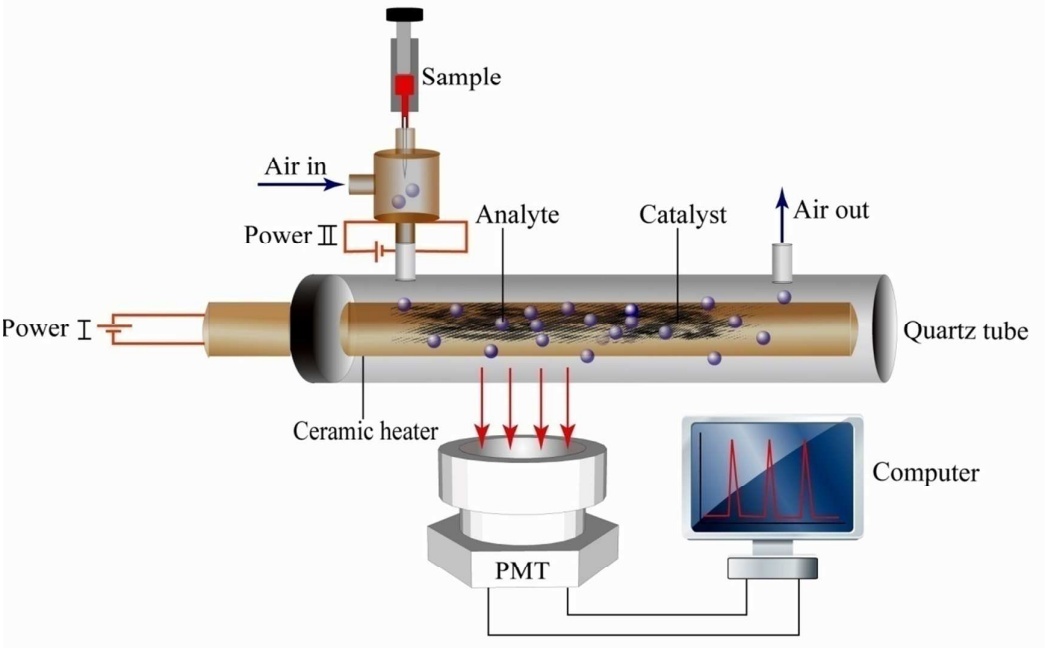

Fig. 1. Schematic diagram of the fabricated sensor device.

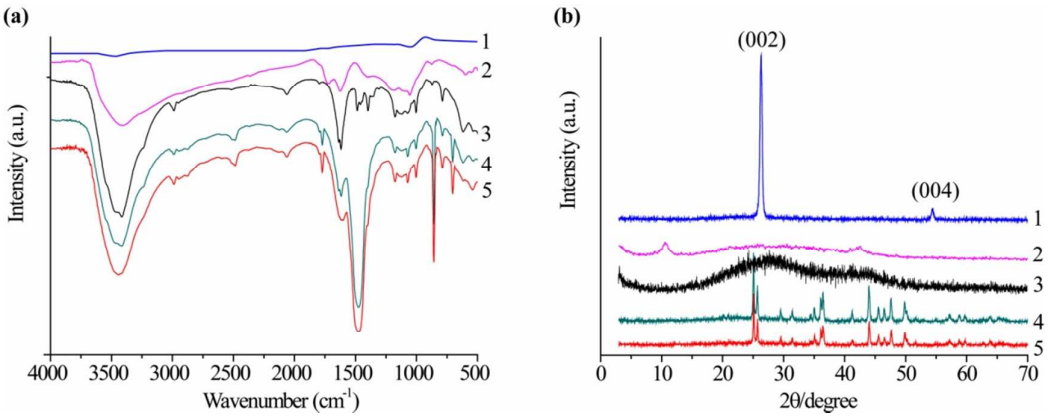

Fig. 2. The FT-IR spectra (a) and XRD patterns (b) of different materials. pristine graphite powder (line 1), GO (line 2), graphene (line 3), $SrCO_3$ (line 4), $SrCO_3$/graphene (line 5).

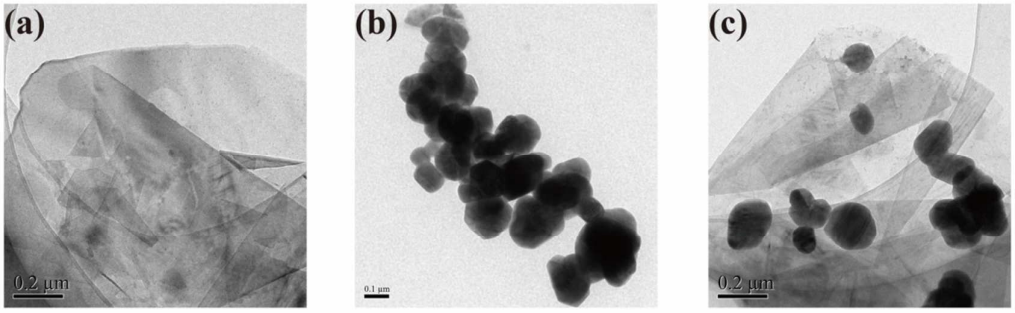

Fig.3. The TEM images of graphene (a), $SrCO_3$ (b), and $SrCO_3$/graphene (c).

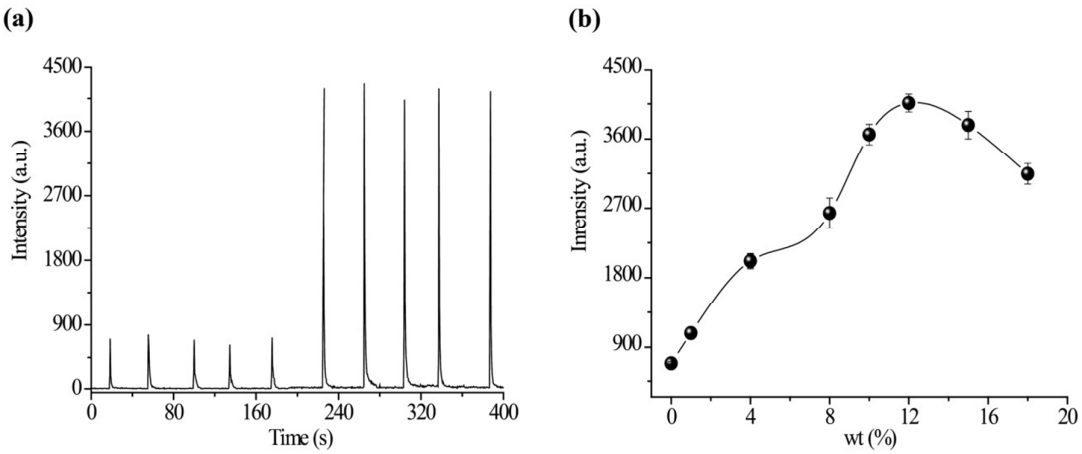

Fig. 4. (a) CTL response for n-propanol on pure $SrCO_3$ and $SrCO_3$/graphene composite; (b) the change trend of CTL intensity for n-propanol versus graphene content. Conditions: detecting temperature, 245 °C; vaporized temperature, 120 °C ; wavelength, 425 nm; air flow rate, 260 mL min^{-1}; concentration of n-propanol is 10 mg L^{-1}. All data points in (b) were run in triplicate.

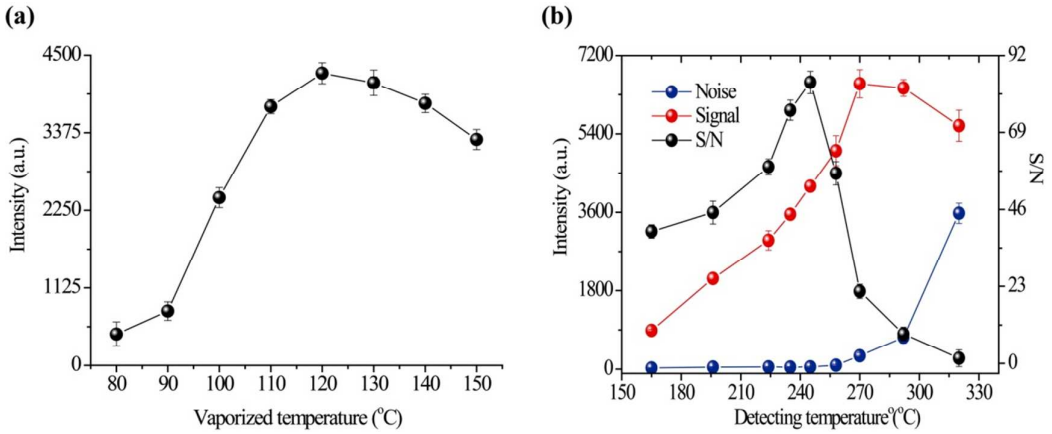

Fig. 5. The change trends of CTL intensity for n-propanol versus (a) vaporized temperature and (b) detecting temperature. Conditions: wavelength, 425 nm; air flow rate, 260 mL min^{-1}; concentration of n-propanol is 10 mg L^{-1}. All data points were run in triplicate.

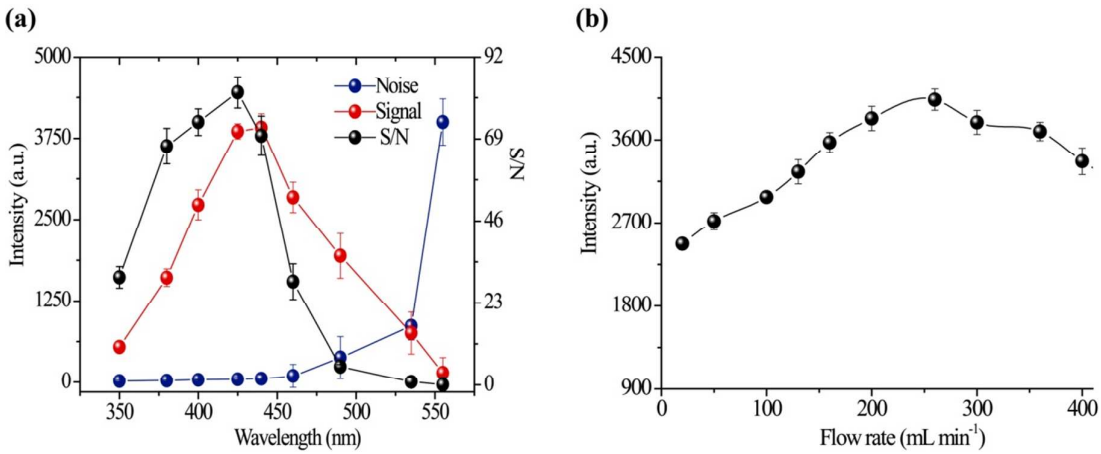

Fig. 6. The change trends of CTL intensity for n-propanol versus (a) wavelength and (b) flow rate. Conditions: detecting temperature, 245 °C; vaporized temperature, 120 °C; concentration of n-propanol is 10 mg L^{-1}. All data points were run in triplicate.

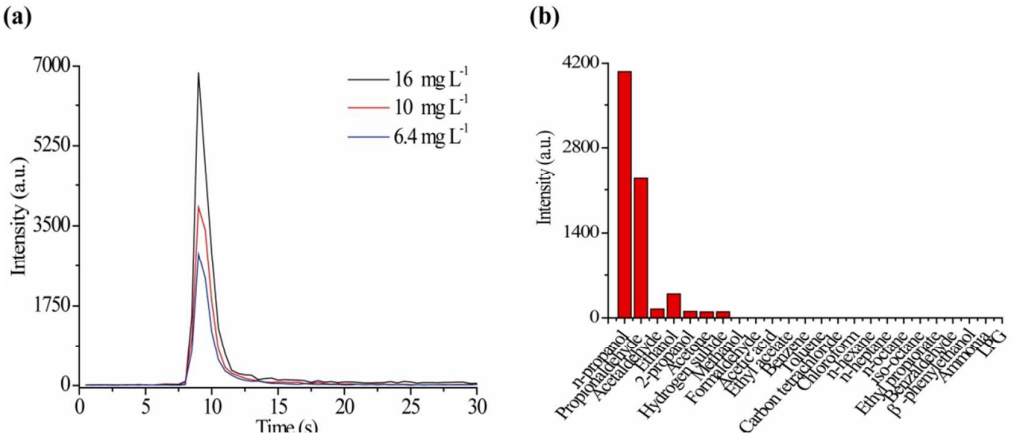

Fig. 7. (a) CTL response curves for different concentrations of n-propanol on $SrCO_3$/graphene composite; (b) sensor response of $SrCO_3$/graphene to different compounds. Conditions: detecting temperature, 245 °C; vaporized temperature, 120 °C; wavelength, 425 nm; air flow rate, 260 mL min^{-1}.

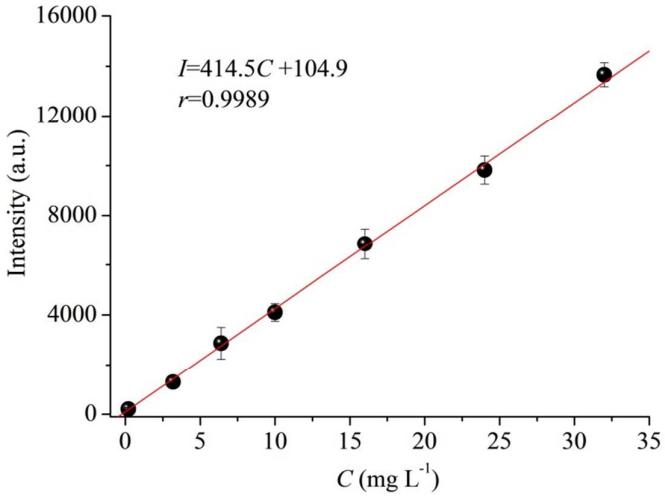

Fig. 8. The calibration curve of n-propanol. Conditions: detecting temperature, 245 °C; vaporized temperature, 120 °C ; wavelength, 425 nm; air flow rate, 260 mL min^{-1}. All data points were run in triplicate.

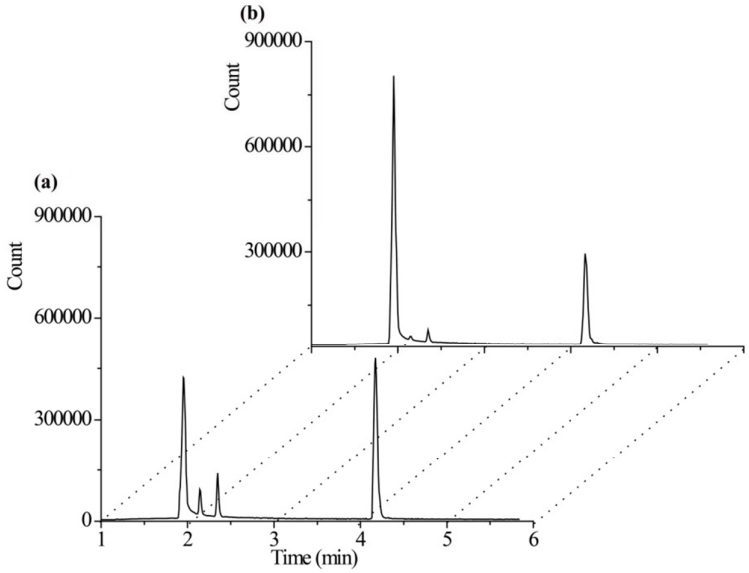

Fig. 9. GC–MS chromatograms from the catalytic products of n-propanol on $SrCO_3$ (a), and $SrCO_3$/graphene composite (b). Carbon dioxide (1.95 min); acetaldehyde (2.15 min); propionaldehyde (2.35 min); n-propanol (4.175 min).

Table 1 Recoveries and precision determined for n-propanol in different samples (n=5).

Sample no.	Spiked concentration (mg L^{-1})					
	1.0		5.0		10.0	
	Re[a] (%)	RSD (%)	Re (%)	RSD (%)	Re (%)	RSD (%)
1	82.4	8.3	88.1	6.6	93.8	5.7
2	116.5	10.4.	107.4	8.8	113.2	6.5

[a]Re: recovery.

Enhanced CTL intensity of n-propanol is observed when adding graphene into $SrCO_3$, which is used for sensitive sensing of n-propanol.